J Mater Sci (2011) 46:1937–1944
DOI 10.1007/s10853-010-5029-8

Shear deformation and grain refinement during accumulative back extrusion of AZ31 magnesium alloy

S. M. Fatemi-Varzaneh · A. Zarei-Hanzaki · S. Izadi

Received: 18 August 2010 / Accepted: 23 October 2010 / Published online: 2 November 2010

Abstract The accumulative back extrusion (ABE), as a new-noble severe plastic deformation (SPD) technique, has been employed to clarify the microstructural evolutions of AZ31 magnesium alloy during severe deformation. The latter has been explored using a 3D finite element analysis along with the microstructural investigations. The distribution of ABE generated shear strain (SS) and its corresponding microstructures have been thoroughly studied. The results indicated that the restrictions of material flow during ABE processing had been led to the mechanical shear bands generation in the microstructure. In addition, the occurrence of continuous dynamic recrystallization (CDRX) within the bands has resulted in a local grain refinement in those areas. Consequently a bimodal structure including the fine recrystallized grains along with the elongated ones has been developed. The effect of deformation mode on the microstructural refinement has been also discussed through considering the developed SS history and the related microstructural refinement.

Introduction

Magnesium alloys as the light structural materials normally exhibit low formability near the room temperature. Accordingly most of the magnesium products are fabricated by casting, in particular, by die casting [1]. In order to exploit the benefits of magnesium alloys, it is important to develop a variety of secondary processing routes which can effectively improve their formability without reducing their strength. As is well known these may be achieved through microstructural grain refinement.

The fabrication of bulk ultrafine-grained (UFG) materials using severe plastic deformation (SPD) methods has attracted a great deal of attention in recent years. This is related to their different engineering advantages in particular high strength and desired ductility at ambient temperature [2–4]. As is well established the shear component of applied plastic strain during SPD processes plays the most effective role in creating the fine grains with high angle grain boundaries [5, 6]. In addition, it is generally accepted that the main mechanism of ECAP grain refinement is solely dictated by the geometry of shear deformation [7]. Lee et al. [6] have also demonstrated that the ultragrain refinement during ARB processing is greatly controlled by the state of applied shear strain (SS). They showed that the grain size distribution through thickness was well synchronized with the SS distributions. The similar results were also reported by Tsuji et al. [8]. Huang et al. [9] have also discussed the role of SS in grain refinement during repetitive corrugation and straightening processing. However, the coincidence of SS and grain refinement in Mg alloys has been rarely focused. Su et al. [7] have related the Mg grain refinement during ECAP to the combination of mechanical shearing and subsequent continuous recovery, recrystallization and growth of grains and subgrains. The clarification of the role of SS in SPD processes is highly important, in particular for deeper understanding of the microstructural evolution during severe deformation of magnesium alloys.

In the present work, the shear strain (SS) distribution, which was introduced by a new-noble SPD process known as accumulative back extrusion (ABE), has been analyzed using a proper finite element (FE) simulation. The

S. M. Fatemi-Varzaneh (✉) · A. Zarei-Hanzaki · S. Izadi
School of Metallurgical and Materials Engineering, University of Tehran, Tehran, Iran
e-mail: mfatemi@ut.ac.ir

aforementioned method has been recently invented and explained by the present authors [10, 11]. In order to verify the simulation results, a special grid method was employed to directly observe the deformation configuration. The microstructural examinations were also performed on the accumulative back extruded material at different process stages to correlate between the developed SS and the achieved grain refinement across the cross-section.

Experimental and simulation procedure

The principle of ABE processing has been thoroughly described elsewhere [10, 11]. A hot-rolled AZ31 magnesium alloy was employed as the experimental and simulation material. The cylindrical testing work pieces were machined in the sizes of ∅18 × 8 mm. The graphite spray was used to reduce the friction between the work piece and the tools surfaces. To directly monitor the SS evolutions during processing, the work pieces were cut into two halves. The square grids with dimension of 1 mm were electro-etched on the face of one half. A clear strain configuration could be observed through utilizing this special technique. The experiments were conducted at 230 °C and ram speed of 10 mm/min. The microstructural examinations were done through common metallographical methods.

The 3D FEM simulations have been carried out analyzing the overall behavior of the specimen in the die. A commercial finite element code Abaqus/Explicit was used to perform all the simulations. An eight-node bilinear plane strain hexahedral (C3D8R) element was employed for the parts. The initial element mesh contains 44,580 elements. The arbitrary Lagrangian–Eulerian (ALE) adaptive meshing, would maintain a high-quality mesh under severe

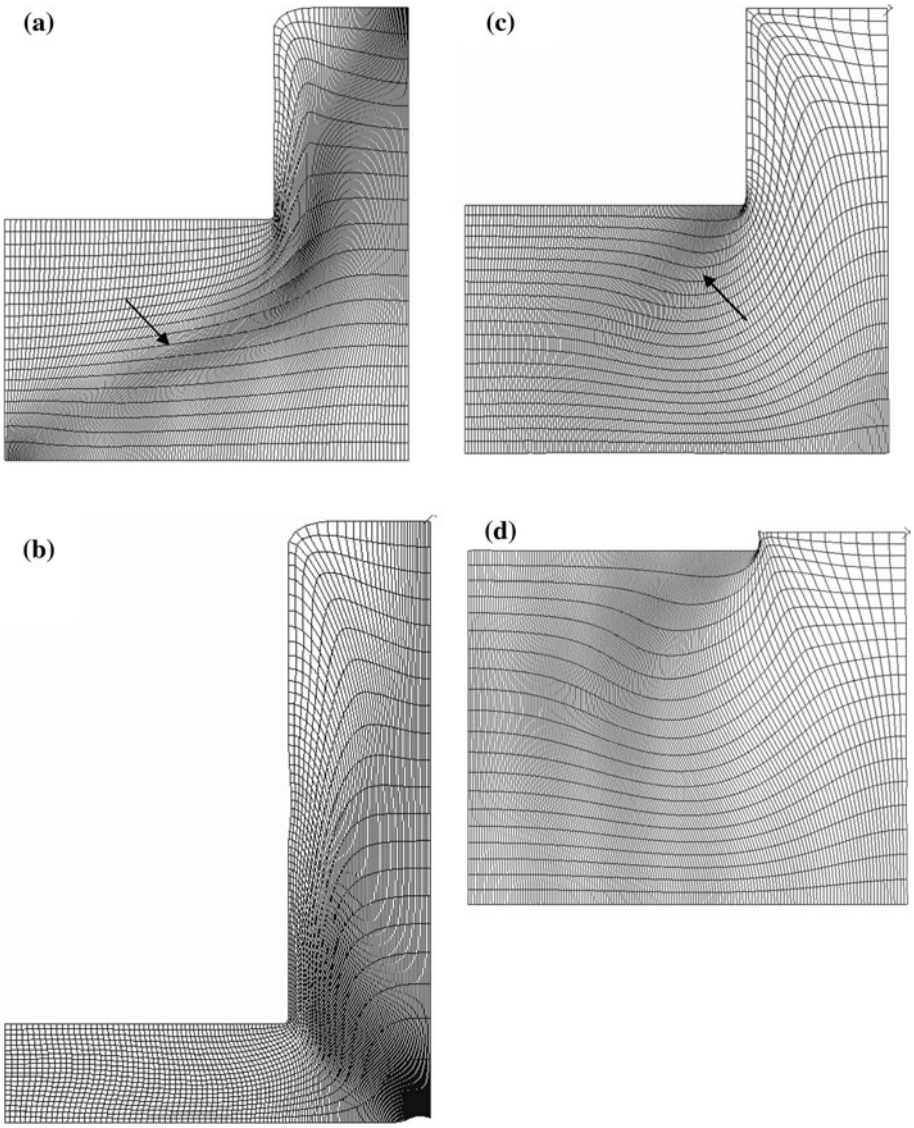

Fig. 1 The FEM-predicted distortion of mesh pattern in AZ31 experimental alloy during **a**, **b** step one; **c**, **d** step two of ABE processing

material deformation by allowing the mesh to move independently with respect to the underlying material. To accommodate the predetermined large strains during simulations the adaptive meshing (automatic remeshing) was employed. A similar cylindrical shape specimen and the Von-Mises yield criterion were adapted for the simulations. The coulomb friction is considered to model the contact between the die and the specimen. The die and the punch were modeled with analytical rigid elements. The friction coefficient (m) was assumed to be 0.15. All the simulations were performed with a speed of 10 mm/min. In order to proceed the simulations, the mechanical properties of AZ31 alloy, which were obtained through hot compression tests [12], and the mechanical properties of a hot worked steel for modeling the punch have been taken into account. The strategy of different point evaluation was selected to examine the evolution of strain and stress in whole specimen.

Results and discussion

Shear deformation behavior

Figure 1 shows the developed mesh pattern during the ABE process. As is observed the deformation mainly

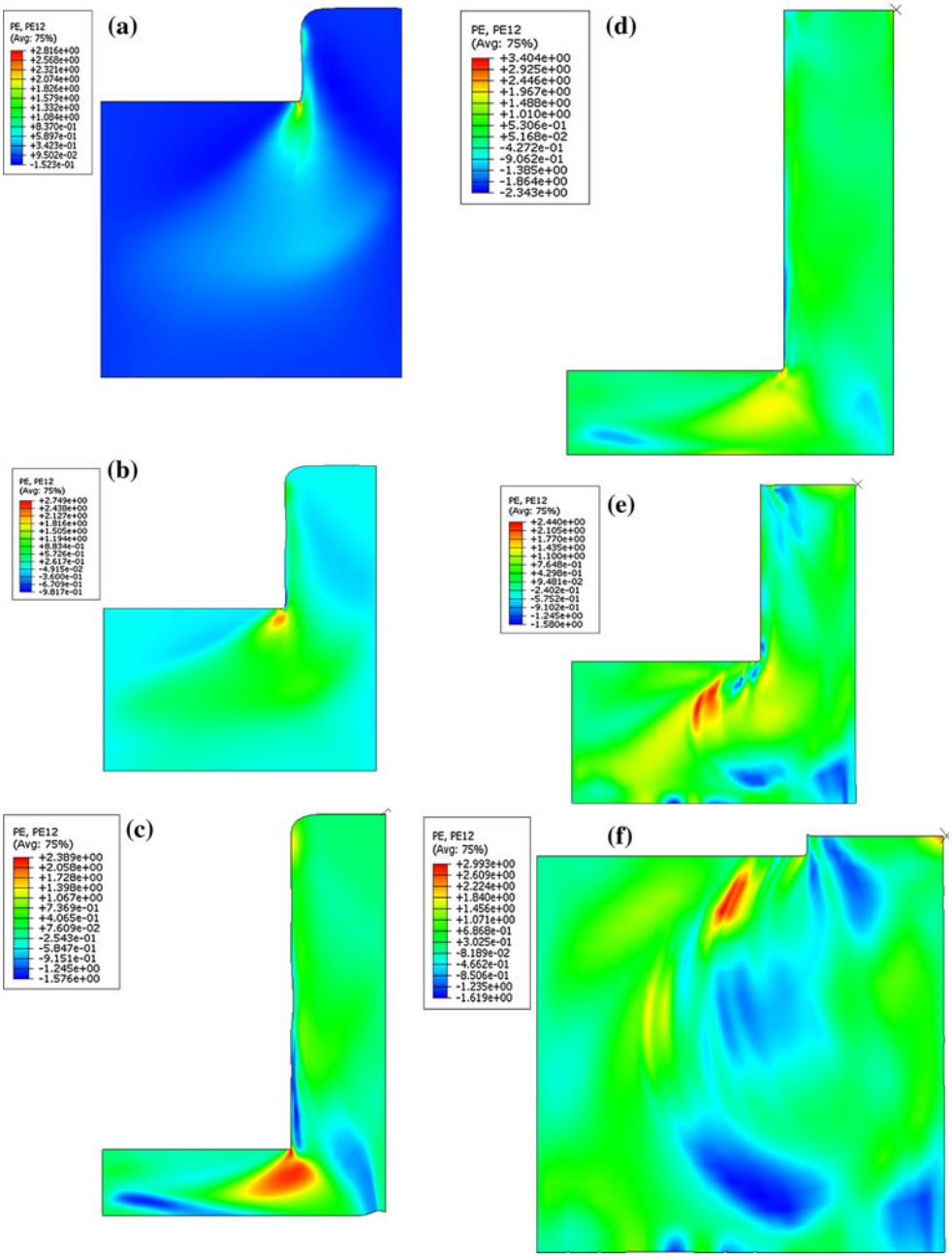

Fig. 2 The shear strain (SS) contours of the AZ31 experimental alloy at different ABE stages (**a–c** step one and **d–f** step two)

demonstrates a simple shear behavior. The highly severe deformation zone may be revealed by analyzing the mesh pattern. A narrow plate-like zone including severe shearing is seen in an inclined position with respect to the punch tip (Fig. 1a, c). The authors consider this region as a pronounced shear plane. It is worth recalling that each pass of ABE processing comprises of two steps (i.e., a back extrusion followed by a forging step) [10]. The material passes the aforementioned zone during the first step and moves concurrently to the wall. The mesh distortions are more homogenous over the cross-section in the second step, where the material flows through a curved route. At the end of process (i.e., after one pass ABE), a distorted mesh pattern with reasonable uniformity is obtained. It has been shown in previous work that ABE technique may impose an equivalent strain of 4–5 after one pass [11].

Figure 2 represents the SS (ε_{12}) contours of the deformed work piece during ABE steps. The results are demonstrated in two dimensions to keep the concerns of axisymmetry and simplicity into consideration. As is seen while the inner punch moves down, the material is deformed by a shear straining scheme toward the gap between the punch and die wall. A channel of shear straining is clearly distinguished through the color difference. As the contours shows the developed SS is almost homogenous all over the affected areas. However, the regions at vicinity of the punch edge, where the amount of strain is significantly raised, the homogeneity reduces. The high values of SS (more than 2) are estimated around the punch edge. The heterogeneity of SS distribution is increased as the process gradually reaches to the end of step one. In contrast, as the second step proceeds the material follows an inverse route where the deformation channel widens as the process approaches to the end of cycle. In comparison to step one, the high values of SS is generated along the boundary where the compressed back material meets the pre-existent one.

P12	P12	P13	P14	P15	P16
P21	P22	P23	P24	P25	P26
P31	P32	P33	P34	P35	P36
P41	P42	P43	P44	P45	P46
P51	P52	P53	P54	P55	P56

Fig. 3 The selected elements in one half of the work piece cross-section

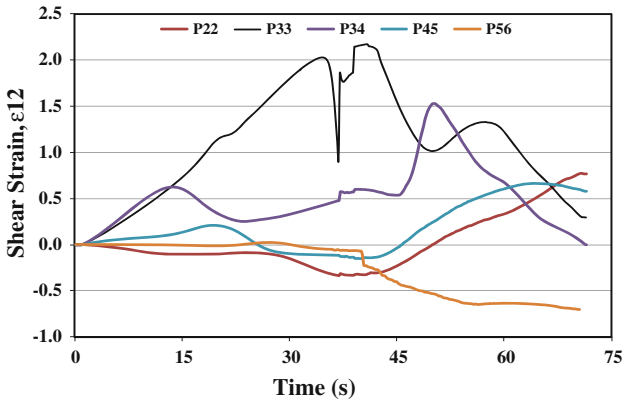

Fig. 4 The variation of shear strains during the ABE processing for typical elements over the cross-section

To follow the deformation history during ABE processing, the SS were analyzed across the cross-section. According to Fig. 3, five typical elements of P22, P33, P34, P45, and P56 were traced to represent the different deformation zones. The variation of SS at various times during the deformation process is shown in Fig. 4. As the results imply, the shear deformation is more effectively imposed on the elements at the center, P33 and P34, during step one. The other elements, however, may not bear a significant amount of SS. This causes an inhomogeneous deformation pattern at the end of step one. As the second step is applied, all the selected elements begin to be effectively deformed by shear deformation. At the end of ABE cycle a reasonable homogeneity may be realized in SS experienced by the elements (Fig. 5).

It should be noted that two adjacent couple of selected elements, i.e., (P22, P33) and (P34, P45) deform via shear straining reversely. In other word, the trend of developed SS is opposite. As the magnitude of SS in one is increased, the other takes a descending behavior and vice versa. The latter is interpreted by the geometry of deformation. The large values of SS may be practically generated at the interfaces of two regions. Considering the limited active slip systems of magnesium alloy, the latter represents itself as the shear bands in the microstructure [13]; this will be discussed later.

Fig. 5 **a** The deformation mesh at initial state; and the deformed mesh at the end of **b** step one, and **c** step two of ABE process

Verification of simulation results

The deformation behavior was examined considering the distortions of the grids plotted on the cross-section by geometrical measurement. The deformed work pieces are shown in Fig. 7. The grids have been gradually deformed during step one (i.e., throughout back extrusion step). However, the distorted grids have been gradually gained their initial shape during the second step. To verify the simulation results a comparison was conducted between the normal strains calculated through simulation method and those of measured ones by grid method. The developed SSs at mid-time in a set of elements along with the deformation axis, i.e., P4j, $j = 1$–6 (the estimated by FEM and the measured ones) are plotted versus the distance from the center line (deformation axis) toward the outer surface of work piece in Fig. 6. As is seen the verification results are qualitatively and quantitatively in a good with simulated ones.

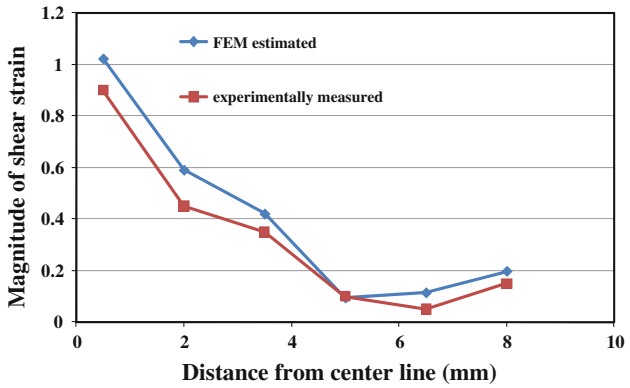

Fig. 6 The shear strain profiles along the P4j ($j = 1$–6) elements of the work piece at deformation mid-time

Shear banding

Generally in all SPD processes the deformation localization is observed through shear band formation. This is considered to be the region of dominant microstructural refinement [14–16]. As is well established if the material work-hardening ability diminishes and the continuous flow becomes unstable, the localized flow commences along the shear bands [14, 17].

The optical metallography on the sectioned work piece at the end of step one, has revealed the important details of deformation behavior of the experimental alloy. The curved shear bands are clearly observed in Fig. 7a, b which interestingly follows the simulated flow pattern. The shear

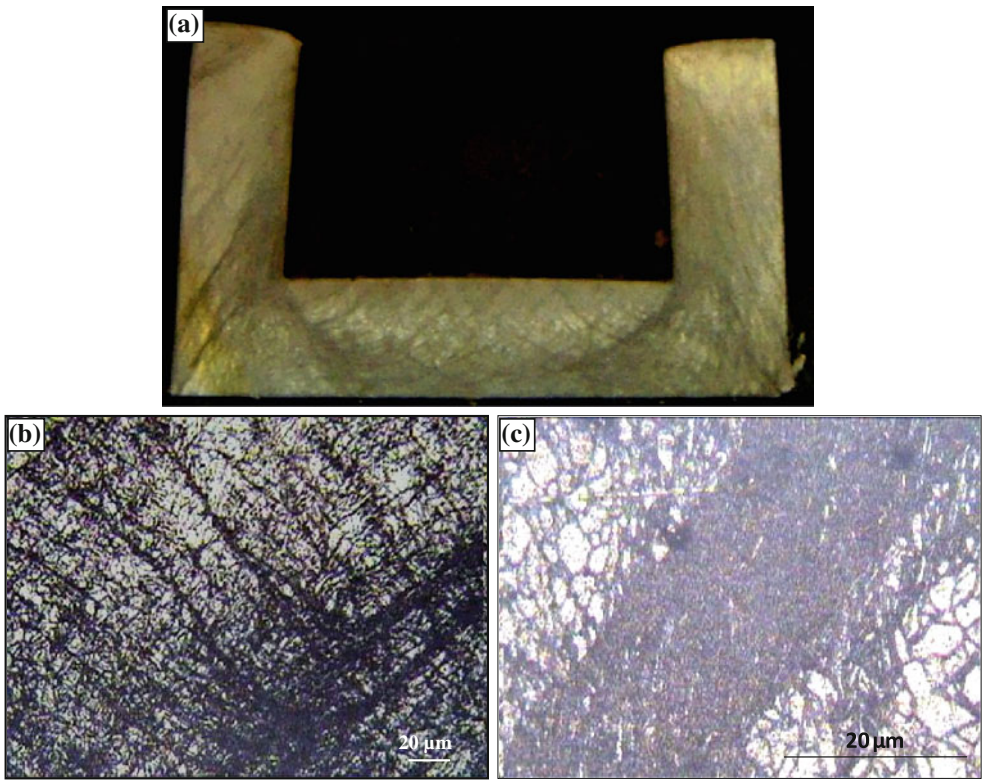

Fig. 7 **a** A low magnification optical micrograph, it shows major shear banding after step one, **b** shear banding at higher magnifications, **c** outstanding grain refinement in shear bands

banding zones along the penetration channel are considerably smaller than those along the wall. The latter may be rationalized by the fact that flow below the punch and along the penetrating channel is much more restricted. It is believed that this restriction creates periodic shear instabilities [18]. In fact the strain energy of deformation is accumulated in shear bands. In contrast to adiabatic shear bands [18], those which are formed during the present unique deformation pattern may be considered as "mechanical shear bands". The latter in fact are produced due to intensive flow localization.

As the back extruded materials (the cup wall) compressed back to the initial shape during step two, the deformation geometry associates with less deformation restriction. Moreover, the fine recrystallized grains which are generated at the end of step one may facilitate the strain hardening of the material during step two, as was also discussed by Lapovok et al. [13]. These two aforementioned reasons lead to continuous and stable flow with less localization during the second step.

Grain refinement

As is seen in Fig. 7c, an outstanding grain refinement is realized in the shear bands. The shearing deformation which is actually achieved inside a shear band is extremely large [18]. This may promote a high density of dislocations followed by continuous dynamic recrystallization (CDRX) [18]. The latter may end up subdividing the bands by high angle grain boundaries through the occurrence of grain refinement. This is consistent with the observation in Mg–Zn–Gd alloy during sever rolling that CDRX took place within the DRX grains and near the shear bands [19]. This mechanism was also denoted during ECAP of AZ31 alloy [20]. However, Guo et al. [21] has reported that CDRX during multiple forging of a cast magnesium alloy is associated with grain splitting due to the formation of microbands that develop in various directions. The occurrence of recrystallization and grain refinement in shear bands has been also discussed by Kaibyshev et al. [22] in aluminum alloys, where grains of 500 nm size was reported to be achieved.

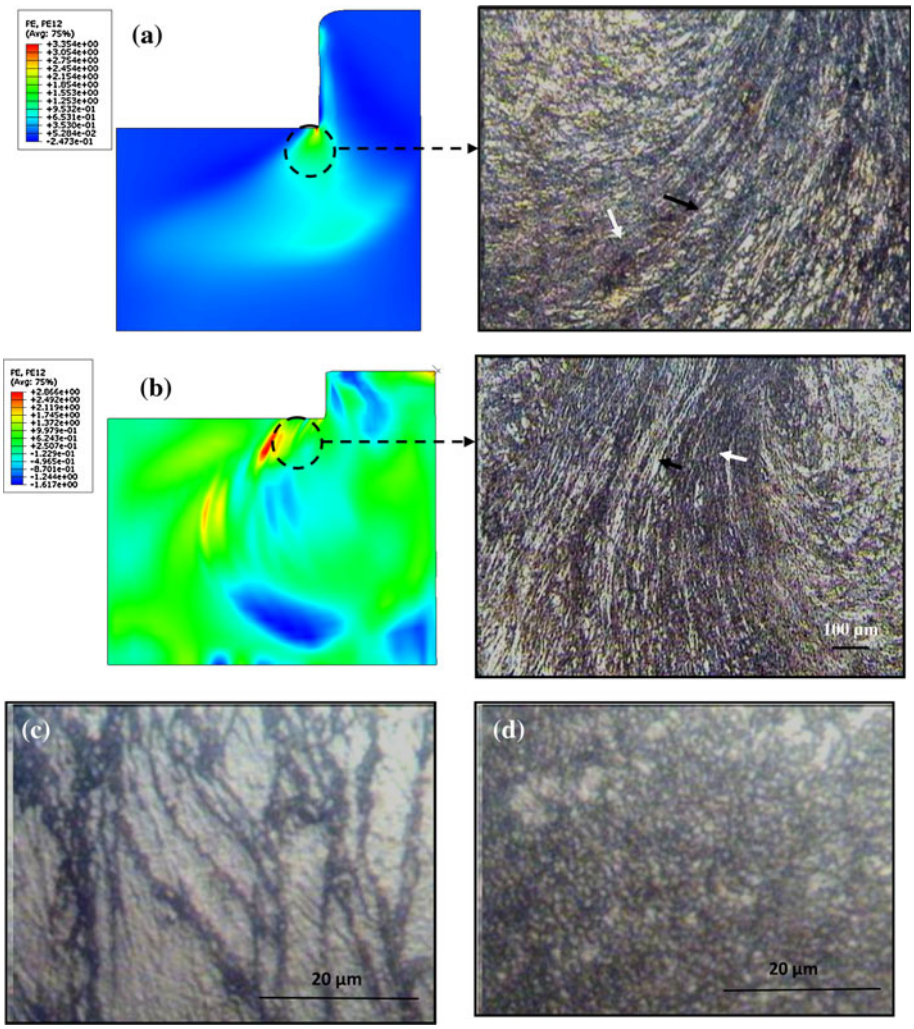

Fig. 8 Optical micrographs and contour maps of SS at the middle stage of **a** step one, **b** step two of ABE where *white* and *black arrows* show the grain refined area, respectively; the microstructures are showing **c** the elongated grains, **d** the fine recrystallized grains

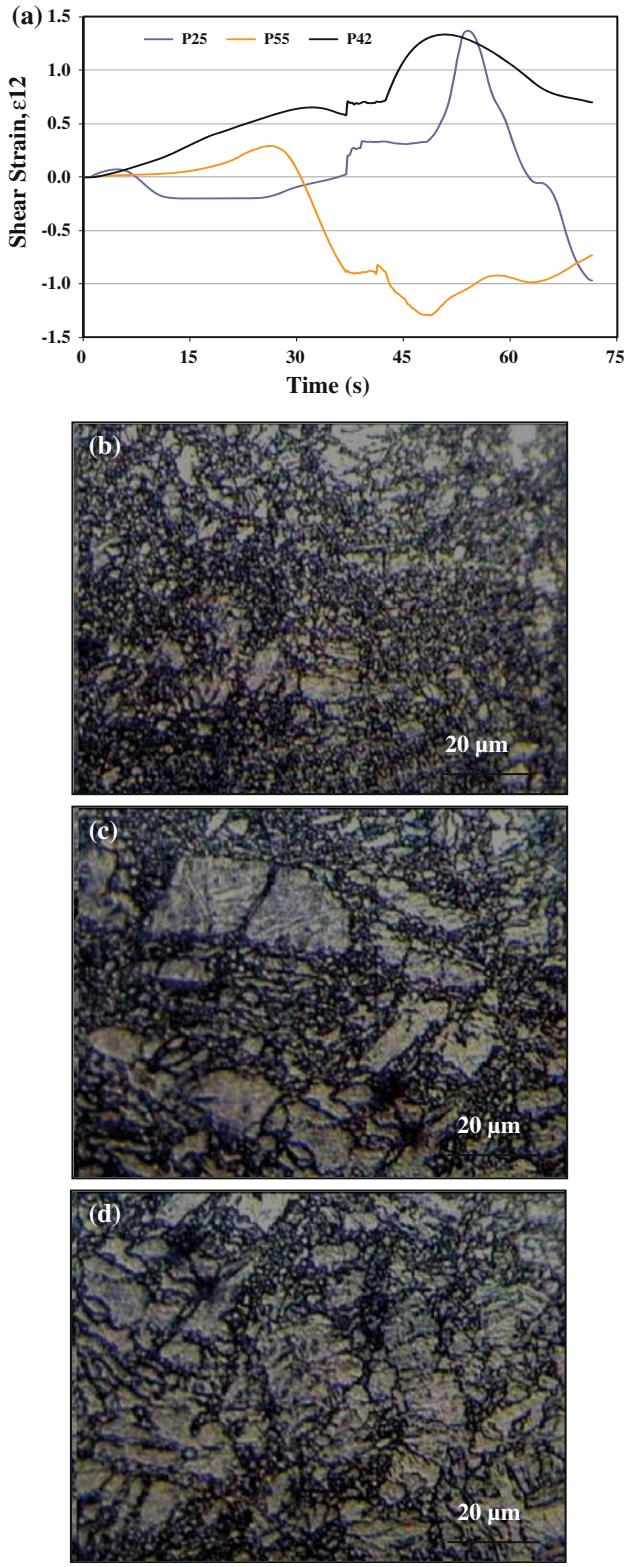

Fig. 9 **a** The variation of SS during the ABE processing for the P25, P55, P42 elements and the related obtained microstructures at **b** P42, **c** P25, and **d** P55

The microstructures of a given position on the work piece cross-section at middle stage of both two steps of deformation and the related SS contours are shown in Fig. 8a and b. A bimodal structure including fine recrystallized grains (Fig. 8c) together with elongated grains (Fig. 8d) are observed at regions inside the deformation channel, where high values of SS are estimated. A mean size of 0.9 μm was measured for the recrystallized grains.

As is well established the mode of deformation is of great importance in grain refinement during deformation processes [16]. SPD processes are very diverse in deformation modes, which may be ranged from pure shear to simple shear. It is believed that the state of simple shear stress is the most effective mode in obtaining UFG materials [16]. In addition the simple shear is the predominant mode in most of SPD processes.

In order to study the mode of deformation three typical elements of P25, P42, and P55 were considered (Fig. 3). The associated SS histories developed in the aforementioned elements during the process are given in Fig. 9a. As is seen, P55 element the deformation history of P55 element is mainly pure shear, while the P42 element is deformed by simple shear. Both of the pure and simple SS modes are present in the deformation history of P25 element. As all three elements were deformed by a similar magnitude of maximum SS, the role of deformation mode in grain refinement may be investigated through comparing the related microstructures of these regions. As is seen (Fig. 9a–c) the higher the share of simple shear in deformation, the more grain refinement is achieved.

As is believed [23] the rotation of unstable orientation to the principal stress may be stimulated under pure shear. Such a rotation may be accompanied by the increase of Schmid factor and texture hardening that delays flow localization. In contrast, the rotation of unstable orientation under simple shear may result in decreasing the Schmid factor and lead to textural softening with early localization [16, 21]. Consequently it is to conclude that the higher share of simple shear in applied deformation may give rise to a more grain refinement through shear banding.

Conclusions

The role of SS and the occurrence of grain refinement during ABE processing of AZ31 alloy has been studied by employing 3D finite element modeling as well as the microstructural examinations. The main conclusions are as follows:

- The SS distribution in the cross-section after step one (back extrusion) is inhomogeneous, whereas it tends to be reasonably homogenous through applying the second step (compression back).
- The strain measurements through grid method present an acceptable conformity with FEM results.
- The mechanical shear bands may be formed during ABE processing due to the restricted material flow. This was shown to closely follow the shearing pattern.
- An outstanding grain refinement was realized in the shear bands. This is believed to be the consequence of continuous dynamic recrystallization and subdividing the bands by high angle grain boundaries.
- A bimodal microstructure including fine recrystallized grains together with elongated grains may be obtained at regions inside the deformation channel, where the high values of SS are predicted.
- The analysis of correlation of the shear deformation path with the related microstructures shows that the higher share of simple shear deformation may give rise to more grain refinement.

References

1. Czerwinski F (2004) Mater Sci Eng A 367:261
2. Tong LB, Zheng MY, Chang H, Hu XS, Wu K, Xu SW, Kamado S, Kojima Y (2009) Mater Sci Eng A 523:289
3. Sabirov I, Estrin Y, Barnett MR, Timokhina I, Hodgson PD (2008) Scripta Mater 58:163
4. Xia K, Wang JT, Wu X, Chen G, Gurvan M (2005) Mater Sci Eng A 410–411:324
5. Shin DH, Kim I, Kim J, Zhu YT (2002) Mater Sci Eng A 334:239
6. Lee SH, Saito Y, Tsuji N, Utsunomiya H, Sakai T (2002) Scripta Mater 46:281
7. Su CW, Lu L, Lai MO (2006) Mater Sci Eng A 434:227
8. Kamikawa N, Sakai T, Tsuji N (2007) Acta Mater 55:5873
9. Huang J, Zhu YT, Alexander DJ, Liao X, Lowe TC, Asaro RJ (2004) Mater Sci Eng A 371:35
10. Fatemi-Varzaneh SM, Zarei-Hanzaki A (2009) Mater Sci Eng A 504:104
11. Fatemi-Varzaneh SM, Zarei-Hanzaki A, Naderi M, Roostaei Ali A (2010) J Alloys Compd 507:207
12. Fatemi-Varzaneh SM, Zarei-Hanzaki A, Haghshenas M (2008) Mater Sci Eng A 497:438
13. Lapovok R, Toth LS, Molinari A, Estrin Y (2009) J Mech Phys Solid 57:122–131
14. MacNalley TR, Swisher DL, Perez-Prado MT (2002) Metall Mater Trans 33A:279
15. Wu PC, Chang CP, Kao PW (2004) Mater Sci Eng A 374:196
16. Segal VM (2002) Mater Sci Eng A 338:331
17. Hirsch J, Lucke K, Hatherly M (1988) Acta Metall 36:2905
18. Murr LE, Trillo EA, Pappu S, Kennedy C (2002) J Mater Sci 37:3337. doi:10.1023/A:1016541023502
19. Yan H, Xu SW, Chen RS, Kamado S, Honma T, Han EH (2010) Scripta Mater (in press)
20. del Valle JA, Ruano OA (2008) Mater Sci Eng A 487:473
21. Guo Q, Yan HG, Chen ZH, Zhang H (2007) Mater Charact 58:162
22. Kaibyshev RO, Mazurina IA, Gromov DA (2006) Met Sci Heat Treatment 48:57
23. Segal VM (2005) Mater Sci Eng A 406:205